Boletim da Sociedade Astronômica Brasileira, **37**, no. 1, 173-176

Dynamical evolution of Large Magellanic Cloud star clusters based on VISCACHA survey observations

J. F. Gardin[1], J.F.C. Santos Jr.[1], F.F.S. Maia[2], B.Dias[3] & B.P.L. Ferreira[4]

[1] DF-ICEX-UFMG, e-mail: joaofranciscogardin12@gmail.com, jsantos@fisica.ufmg.br
[2] IF-UFRJ, e-mail: ffsmaia@if.ufrj.br
[3] IA-FCE-UNAB/Chile, e-mail: astro.bdias@gmail.com
[4] IAG-USP, e-mail: plfbernardo@gmail.com

Abstract. This study analyzes high-quality photometric data from the VISCACHA Survey in the LMC by fitting stellar density profiles with a family of lowered isothermal models. After applying a completeness correction and adopting physical distances and ages, it was possible to determine the clusters' kinematical and structural properties directly from the photometric catalogs. The dynamical and half-relaxation timescales of the clusters were then computed to quantify their degree of dynamical evolution expressed by the dynamical age. It is indicated that the dynamical age correlates with the internal potential and the clusters' half-mass radii, and appear to be independent of the location in the galaxy.

Resumo. O presente estudo analisa dados fotométricos de alta qualidade do projeto VISCACHA na GNM através de ajustes dos perfis de densidade radias usando uma família de modelos isotérmicos reduzidos. Após aplicar uma correção de completeza e adotar valores físicos de distância e idade, foi possível determinar as propriedades dinâmicas e estruturais dos aglomerados diretamente dos catálogos fotométricos. As escalas de tempo dinâmicas e de meia relaxação foram computadas para quantificar o grau de evolução dinâmica, expressada através da idade dinâmica. É indicado que a idade dinâmica correlacione com o potencial interno e o raio a meia massa do aglomerado, sendo aparentemente independente da localização na galáxia.

Keywords. Galaxies: star clusters: general – Magellanic Clouds – Surveys

1. Introduction

The Magellanic Clouds (MCs) are the closest example of a pair of binary, interacting galaxies and also the largest satellites of the Milky Way. Their proximity and location in the sky enable detailed observations of their stellar populations. Their history of interaction and close encounters have produced an interesting environment for the study of the formation and evolution of their stellar clusters. The low density medium in the MCs (when compared to the Milky Way) may also contribute to cluster longevity, allowing many systems to survive for longer timescales.

Within this context, the VISCACHA Survey (Maia et al. (2019), http://www.astro.iag.usp.br/~viscacha/) is an ongoing project based on high-quality, deep photometric observations of star clusters in the MCs. Focusing on peripheral clusters and in the bridge, where the background contamination is lower, the Survey uses the SOAR telescope, with the instrument SAMI, which improves the observations seeing (Tokovinin et al. (2016)). The project aims to deliver homogeneous BVI photometry reaching as deep as $V \approx 24$, enabling the analysis of faint stellar populations.

In this work, we investigate the structural and dynamical evolution of 85 clusters in the periphery of the Large Magellanic Cloud (LMC), using the photometric catalogs from the VISCACHA Survey. After a completeness analysis, we characterize the clusters' spatial structure and dynamical state and evaluate their timescales by combining the photometric information with previously derived distances and ages. Figure 1 shows the spatial distribution of the clusters studied in this work.

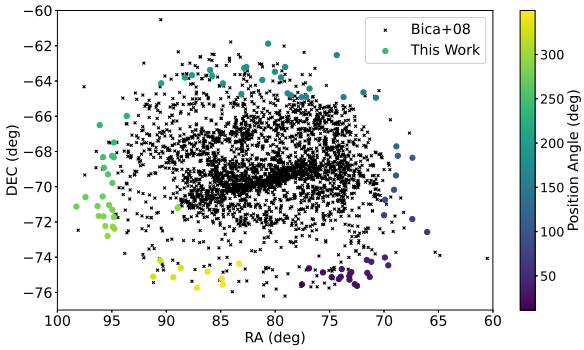

Figure 1. Spatial distribution of LMC star clusters catalogued by Bica+08 (black crosses). The clusters studied in this work are marked with coloured circles, where their color reflect their position angle in relation to the LMC center, as indicated in the colorbar.

2. Methodology

2.1. Photometric Completeness

Since our analysis relies exclusively on stellar counts extracted from the photometric catalogs, it is essential to determine the completeness of the detected stars. This quantity is an estimate of the fraction of stars that are missing from the final processed images and catalogs due to instrumental limitations, crowding, visual alignment or saturation.

To estimate the completeness, we will adopt the methodology described in Gardin et al. (2024), which measures the completeness using the photometric catalogs, without needing the images. The method consists on the creation of articial star grids with uni-

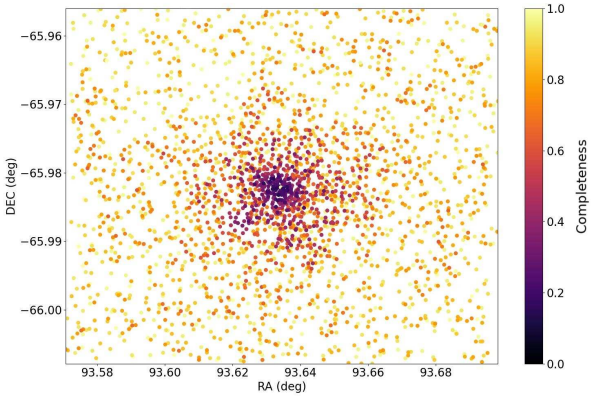

Figure 2. Spatial distribution of all observed star in the SAMI field of view of the cluster SL866. The colors represent their completeness in the I band.

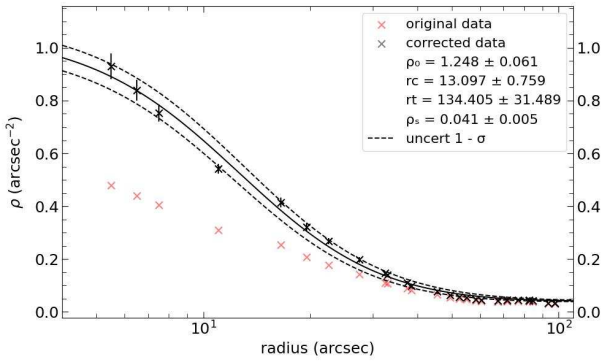

Figure 3. RDPs for the cluster SL866. Red crosses are the raw stellar surface densities, while black crosses show the completeness corrected profile. The empirical King model is fitted to the corrected profile.

formly spaced magnitudes covering the full field of view of the observations. For each artificial star, the distance to the nearest observed star in the catalog is computed, and the magnitudes of the artificial and observed stars are compared. Depending on these spatial and photometric factors, the artificial star is said to be recovered or not.

From the photometric residual images, we flag all regions affected by saturated stars, bleeding trails, bad pixels, or extended sources to yield zero completeness because artificial stars placed in these regions will not be matched to real detections. Finally the local completeness at a given magnitude and position is defined as the fraction of artificial stars in that bin (in position–magnitude space) that are recovered. By doing this for a range of magnitudes and grid densities, completeness map across the entire field and magnitude range is built.

Once the completeness grid for the artificial stars is constructed, interpolation is used to assign a completeness value to each observed star based on its magnitude and location. These completeness will then be used in the subsequent analyses. Figure 2 illustrates the resulting completeness distribution for the cluster SL866.

2.2. Structural and Dynamical Properties

After estimating the completeness for each cluster, we created radial density profiles (RDPs) using both the observed number of stars and the completeness corrected number of stars. To prevent an artificial over correction of the stellar densities in highly incomplete regions, we imposed a lower completeness limit to 0.5. This ensures that one observed star can only generated at most one additional star.

We first fit the empirical King (1962) profile to the completeness corrected RDPs, given by:

$$\rho(r) = \rho_0 \left[\frac{1}{\sqrt{1+(r/r_c)^2}} - \frac{1}{\sqrt{1+(r_t/r_c)^2}} \right]^2 + \rho_{bg}, \quad (1)$$

from which we derived the core radius r_c, tidal radius r_t and the central projected density of stars ρ_0. The background density ρ_{bg} was estimated from the outer regions of the field.

The completeness has a stronger effect in the determination of the core radius than on the tidal radius. The central regions are most affected by crowding and unresolved mergers, which lowers the completeness compared to the outer regions where the stellar density is low and the completeness is most affected by the photometric limit rather than star contamination. Figure 3 shows the RDPs and fit for the cluster SL866.

After the empirical fit we performed an additional series of fits using a family of lowered isothermal models implemented through the Lowered Isothermal Model Explorer in PYthon (`LIMEPY`) code (Gieles & Zocchi (2015), `https://github.com/mgieles/limepy`). The `LIMEPY` models form a self-consistent, spherical suite of distribution function (DF) based models that generalize classical lowered isothermal profiles such as Woolley (1954), King (1966) and Wilson (1975) models by allowing the tuning of the truncation parameter g of the energy distribution.

For isotropic, single-mass models, the distribution function is:

$$f(E) = A\mathcal{E}_\gamma(g, \hat{E}), \quad (2)$$

where $\hat{E} \equiv \phi_t - E/s^2$ is the reduced energy, A is a normalization constant, and s is the model velocity scale. The function $\mathcal{E}_\gamma$ is defined as:

$$\mathcal{E}_\gamma(g, \hat{E}) = \begin{cases} \exp(\hat{E}), & g = 0 \\ \exp(\hat{E})\frac{\gamma(g,\hat{E})}{\Gamma(g)}, & g > 0 \end{cases} \quad (3)$$

where $\gamma(g, \hat{E})/\Gamma(g)$ is the regularized lower incomplete gamma function. The special cases where $g = 0, 1, 2$ return the known Woolley (1954), King (1966) and Wilson (1975) models, respectively.

`LIMEPY` can return its models either in dimensionless units or in physical units, depending on the user input of the scale radius. Therefore, to work with physical units, we adopted distances and ages derived with the `SIESTA` code (Ferreira et al. (2024), `https://github.com/Bereira/SIESTA/`), which performs a statistical matching between color-magnitude diagrams of real and synthetic stellar populations, Using these distances, we converted the completeness corrected RDPs to physical units and fitted a set of `LIMEPY` models.

For each cluster, we computed a series of `LIMEPY` models spanning the parameter space in central potential W_0, scale radius r_0, total mass M and g. We then fit these models in parameter space to get the one that had the minimum χ^2 relative to the observed profile. Figure 4 shows the fitted models for the cluster SL866.

From the best-fitting model we extracted all parameters r_0, r_h and r_t in parsecs and M in solar masses. Since `LIMEPY` is parameterized by the dimensionless central potential W_0, its value

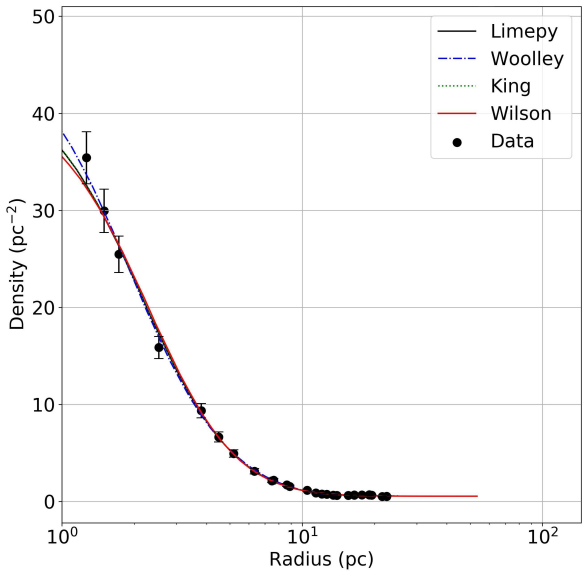

Figure 4. Completeness corrected RDP for the cluster SL866 in physical units with dynamical fits obtained using LIMEPY. Models with fixed truncation parameters $g = 0, 1, 2$ correspond to the Woolley, King, and Wilson models, respectively, and are shown together with the fit where g is treated as a free parameter, indicated as LIMEPY.

is also obtained from the best-fitted model and will serve as the estimate of the cluster central potential.

2.2.1. Dynamic Evolution and Timescales

In order to characterize the internal dynamical state of the clusters, we need to compute timescales derived their dynamical parameters. These timescales will allow us to quantify the degree of evolution of the clusters and compare different clusters.

The first relevant quantity is the crossing time, t_{cr}, which measures the time that a star takes to move across the cluster radius. Using the half-mass radius r_h as scale, it can be approximated as:

$$t_{cr} \sim \sqrt{\frac{r_h^3}{GM}}, \tag{4}$$

where G is the gravitational constant and M is the cluster mass.

The second timescale is the half-relaxation t_{rh}. This is an estimate of the time that a star takes to lose all memory of its initial orbit due to the sufficient 2 body gravitational encounters along its life in the cluster. Following Binney & Tremaine (2008) formulation, it can be written as:

$$t_{rh} = \frac{2.06 \times 10^6}{ln(0.4M/< m >}\sqrt{\frac{Mr_h^3}{< m >^2}}, \tag{5}$$

where $< m >$ is the mean stellar mass of the cluster. The relaxation time generally increases with both the cluster mass and its characteristic size, and decreases for systems composed of lower-mass stars, due to their higher encounter rate.

We can finally quantify the degree of dynamical evolution of the cluster through its dynamical age:

$$t_{dyn} = age/t_{rh}, \tag{6}$$

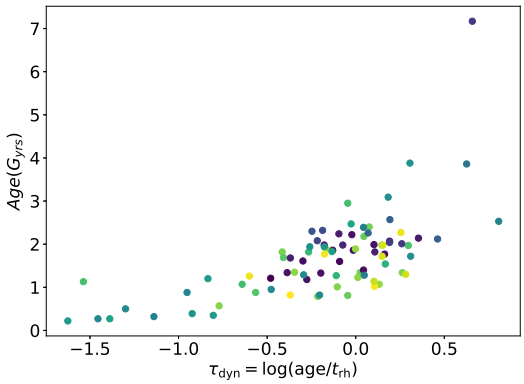

Figure 5. Relation between chronological age and dynamical age for all clusters in this study. The colors represent the position angle as in figure 1.

which relates the cluster's chronological age to its relaxation timescale. We calculated the dynamical age of all clusters utilizing the ages derived from the SIESTA code and the dynamical parameters obtained from our LIMEPY analysis. Figure 5 shows the relation between age and dynamical age for all clusters analyzed.

We adopted a fixed mean stellar mass of $< m >= 0.5 M_\odot$ when determining the half relaxation times. We choose this value because it is consistent with the mean stellar mass in the Milky Way evolved clusters (Baumgardt & Makino (2003)) and is also consistent with our use of single-mass, isotropic models. Since we treat all clusters in our sample in the same way, the choice of $< m >$ does not influence the comparisons that we wish to analyze. Different values will only produce a uniform shift in the plots.

It is important to state that the dynamical masses recovered from the LIMEPY fits correspond only to the portion of the mass traced by stars brighter than the preset limit. The dynamical and structural parameters are not biased by this limit since we assume that the cluster has no mass segregation. We avoid fitting the profiles beyond the photometric limit because completeness corrections become less reliable in the regime where the number of detected stars is too low.

3. Results

The figure 6 summarizes the main results of this study. The distribution of dynamical ages are more spread among clusters in the northern region of the LMC and clusters in the south appear to occupy a smaller range of dynamical states.

For the entire sample, the clusters appear to shrink toward smaller half-mass radii with increasing dynamical age. In other words, more dynamically evolved clusters appear to be systematically more compact. This trend is visible in the whole sample, but it is noticeably steeper for clusters in the southern region (purple and yellow points).

The central potential W_0 displays greater scatter and spread values at low dynamical age ($\tau \approx 0$). Despite this, it appears as a general trend that there is a decline of W_0 with increasing dynamical age, which is consistent with the gradual depletion of bound stars as clusters evolve. This effect is more apparent on clusters in the northern region (near $PA \approx 200°$).

In summary, the clusters half-mass radii decrease with increasing dynamical age, indicating that the clusters contract along their evolution. The central potential tends to also decrease with

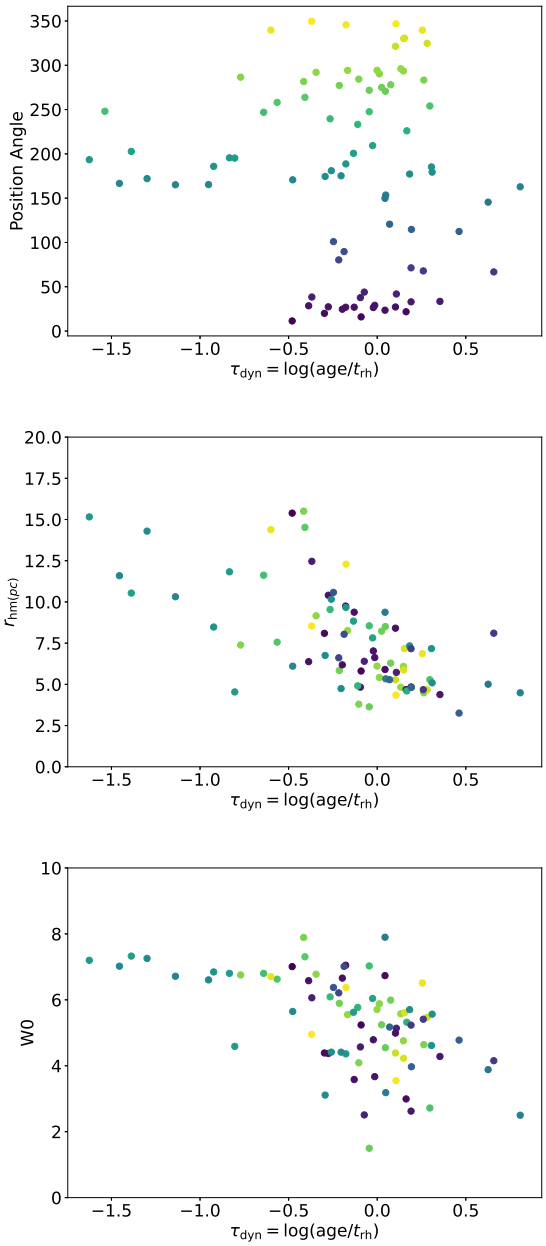

Figure 6. Top pannel: relation between the studied clusters dynamical age and their position angle related to the center of the LMC. Middle pannel: relation between the half mass radius and the dynamical age. Bottom pannel: relation between the clusters central potential and their dynamical age. The colors represent the position angle as in figure 1.

evolution, indicating that clusters are losing binding energy over time.

The location of the cluster in the galaxy does not appear to influence their evolution. The bigger spread in the dynamical ages of the clusters in the northern region when compared to the others might be related more to their greater range of chronological ages than to their position, as we can see in figure 5.

4. Conclusions

The dynamical parameters derived for the studied objects indicate that the evolution of the clusters in the outskirts of the LMC is primarily governed by their internal relaxation. Even though the clusters may be subjected to external perturbations and tidal interactions with the SMC and the Milky Way, these effects appear to not have a greater influence in the overall dynamical evolution of the clusters.

A methodological limitation of the method is that we used a single mean mass for the entire sample of clusters. Even though this assumption introduces only a small shift in the dynamical age, it assumes that all clusters have the same mean mass. Given this, a more complete follow up to this work is to estimate the total mass of the clusters through extrapolation of the observed mass function and then recalculate the mean mass and the dynamical age of the clusters.

Acknowledgements. We thank the Conselho Nacional de Desenvolvimento Científico e Tecnológico (CNPq) and the Coordenação de Aperfeiçoamento de Pessoal de Nível Superior (CAPES) for the partial financial support to this project.

References

Baumgardt H. & Makino J. (2003), MNRAS, 340, 227
Bica E., Bonatto C., Dutra C. M., et al. 2008, MNRAS, 389, 678
Binney J., Tremaine S. 2008, Galactic Dynamics: Second Edition, Princeton University Press, Princeton
Ferreira B. P. L, Santos Jr. J. F. C., Dias B. et al. 2024, MNRAS 533, 4210
Gardin J. F., Santos Jr. J. F. C., Maia F. F. S. et al. 2024, MNRAS, 532, 1683
Gieles M. & Zocchi A. 2015, MNRAS, 454, 576
King I. 1962, AJ, 67, 471
King I. 1966, AJ, 71, 64
Maia F. F. S., Dias B., Santos Jr. J. F. C. et al. 2019, MNRAS, 484, 5702
Tokovinin A., Cantarutti R., Tighe R. et al. 2016, PASP, 128, 125003
Wilson C. P. 1975, AJ, 80, 175
Woolley, R. V. D. R. 1954, MNRAS, 114, 191